Supplementary Material

Single Atom Fe-Based Catalyst Derived from the Hierarchical (Fe,N)-ZIF-8/CNFs for High-Efficient ORR Activity

Wenfang Miao[a], Feirong Huang[a], Xiaochen Shen[a], Shaopeng Li[a], Xingru Cao[a], Xuefeng Zhang[b], Jieyi Yu[b] and Xinglong Dong[a]**

[a]*Key Laboratory of Materials Modification by Laser, Ion and Electron Beams (Ministry of Education), School of Materials Science and Engineering, Dalian University of Technology, Dalian 116024, China.*

[b]*Institute of Advanced Magnetic Materials, College of Materials and Environmental Engineering, Hangzhou Dianzi University, Hangzhou 110819, China.*

[*]*Corresponding authors.*

E-mail addresses: yujieyi@hdu.edu.cn, dongxl@dlut.edu.cn

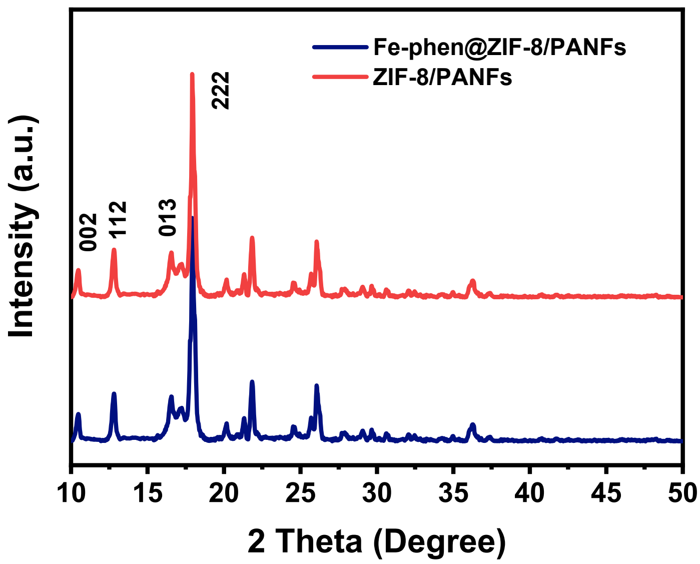

Fig. S1. XRD patterns of ZIF-8/PANFs and Fe-Phen@ZIF-8/PANFs.

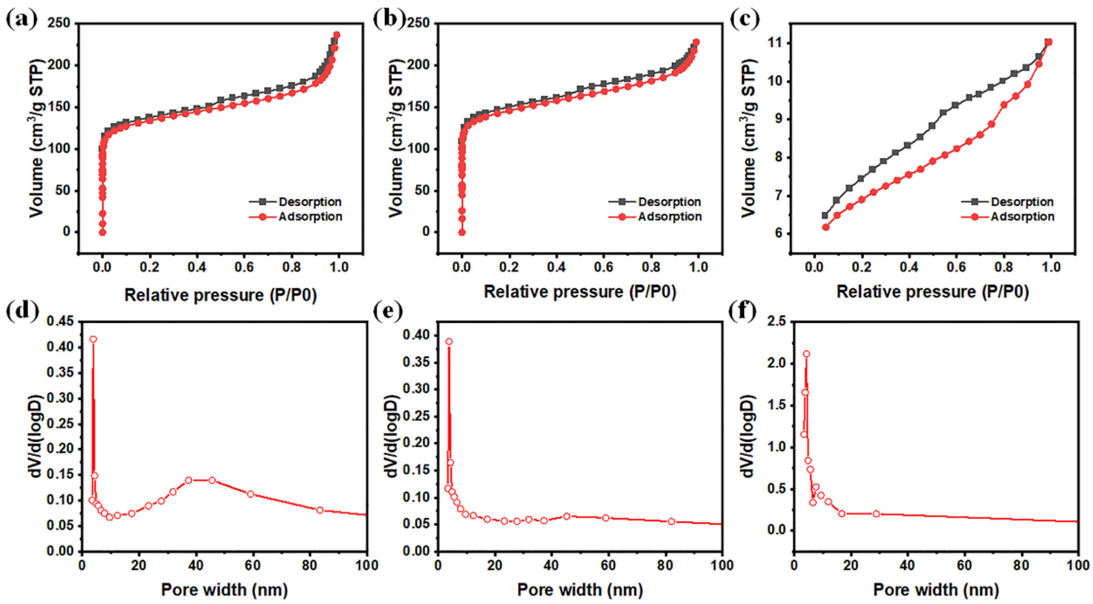

Fig. S2. (a-c) N_2 adsorption-desorption isotherms, and (d-f) the corresponding pore size distribution of the Fe-N*x*-CNFs, the N*x*-CNFs and the CNFs.

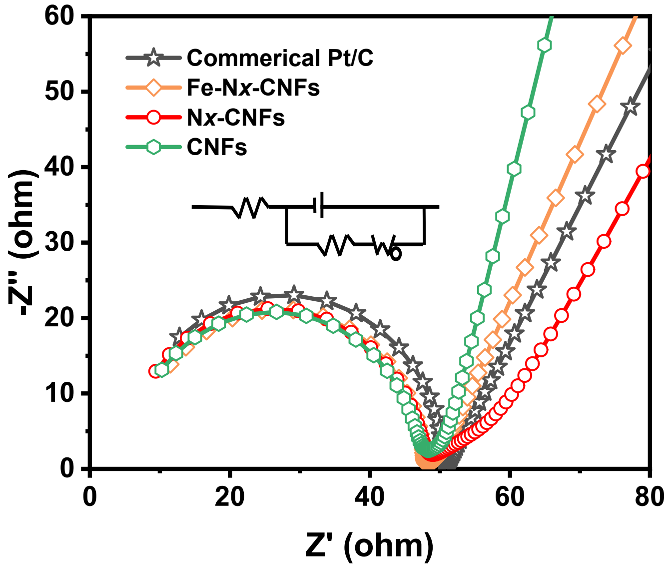

Fig. S3. EIS (Nyquist plots) of commercial Pt/C, Fe-N*x*-CNFs, N*x*-CNFs and CNFs samples.

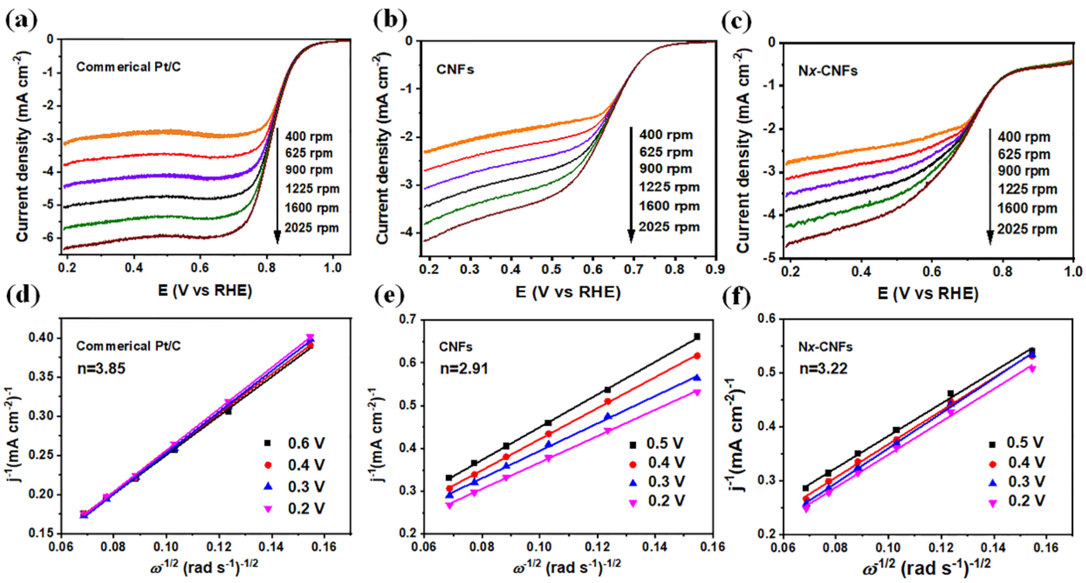

Fig. S4. Voltammograms of (a) commercial Pt/C; (b) CNFs; (c)N*x*-CNFs at various speeds at a scan rate of 10 mV s^{-1}; and (d-f) are the corresponding K–L plots at different potentials.

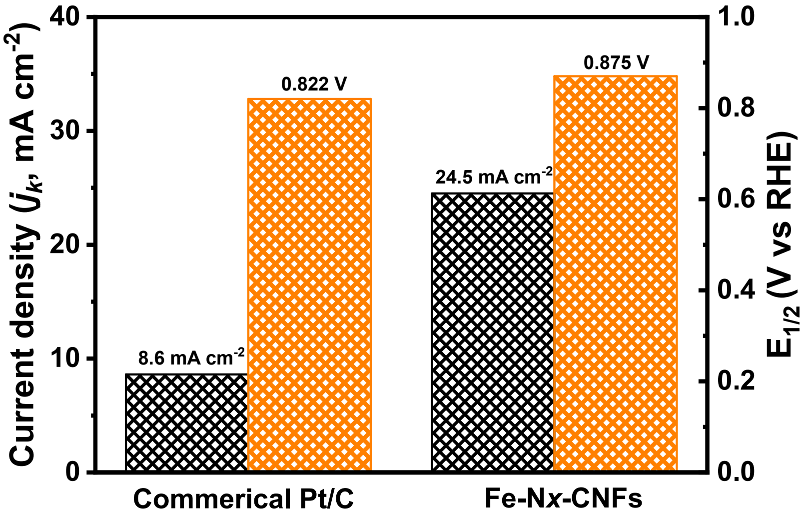

Fig. S5. The kinetic current densities (J_k) at 0.8 V and $E_{1/2}$ of the commercial Pt/C and the Fe-N*x*-CNFs.

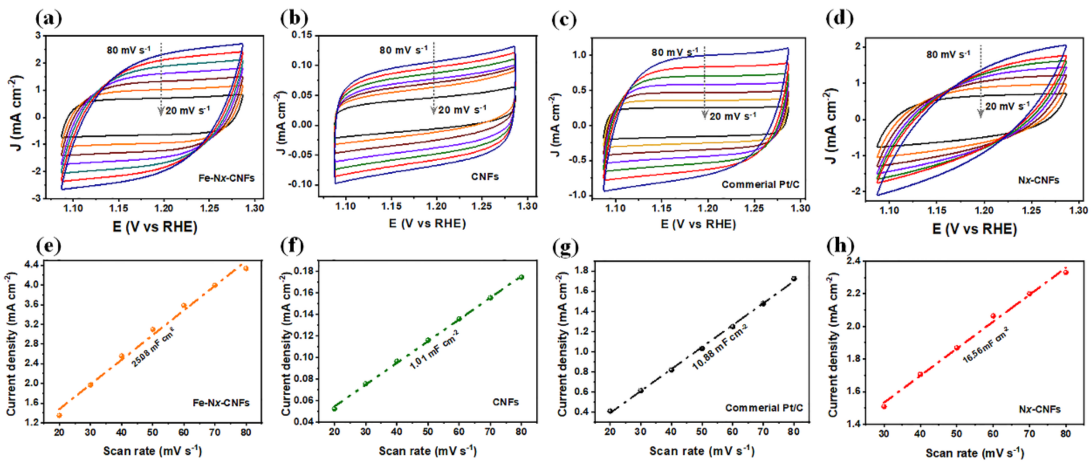

Fig. S6. The CV curves at different scan rates (20-80 mV s^{-1}), in N_2-Saturated 0.1M KOH and corresponding C_{dl} of the samples.

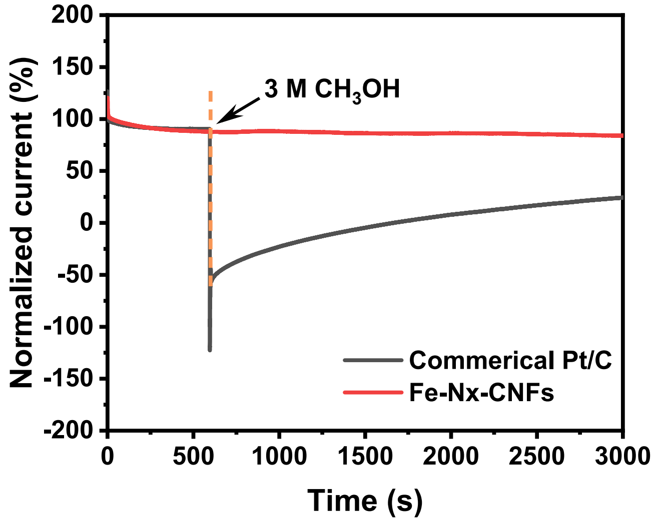

Fig. S7. Methanol resistance test of the Fe-Nx-CNFs and the commercial Pt/C.

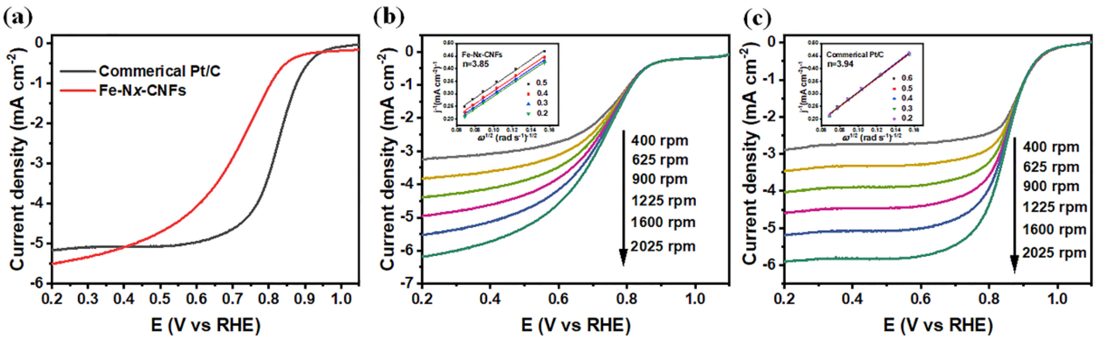

Fig. S8. (a) ORR polarization curves of the Fe-Nx-CNFs and the commercial Pt/C in oxygen saturated 0.1 M $HClO_4$ at a rotating rate of 1600 rpm. LSV curves of (b) Fe-Nx-CNFs and (c) commercial Pt/C at different rotating rates in oxygen saturated 0.1 M $HClO_4$and the corresponding K-L plotsand the calculated electron transfer (inset).

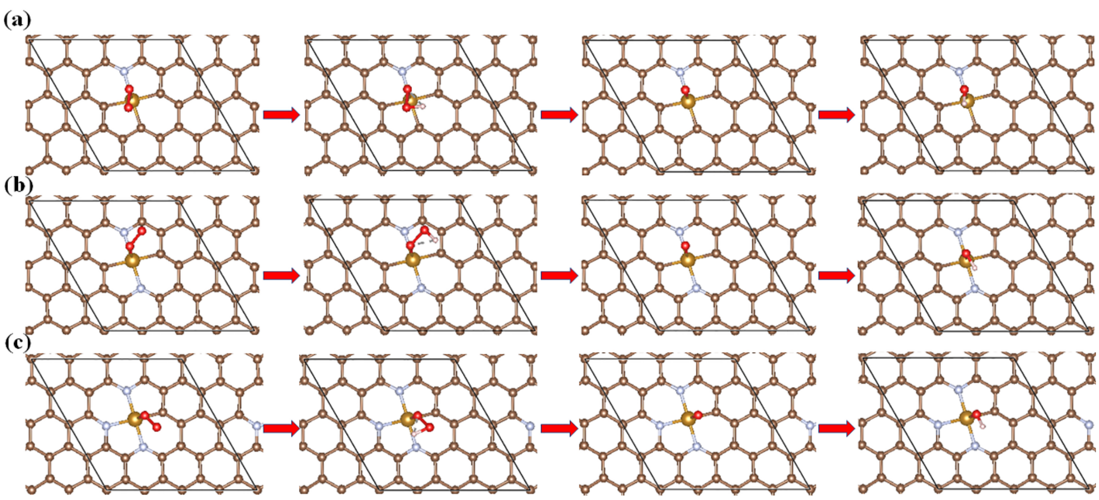

Fig. S9. ORR mechanisms over (a) FeN_1; (b) FeN_2; and (c)FeN_3 active site. The central atom is Fe; brown, silver, red and white balls represent the C, N, O and H atom, respectively.

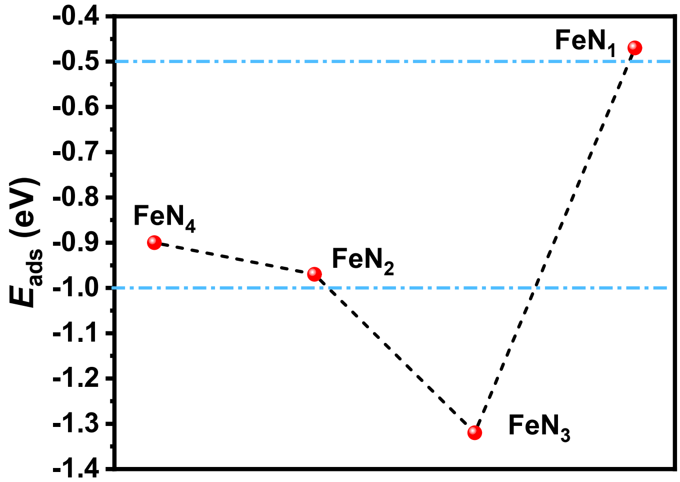

Fig. S10. The adsorption energy of FeN_{1-4}.

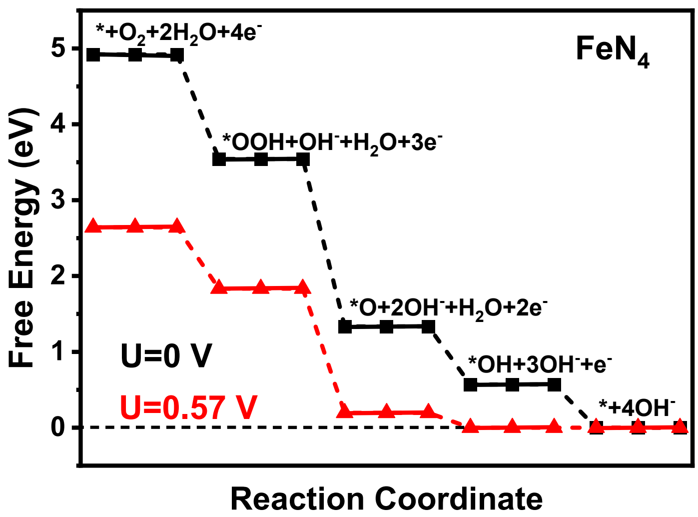

Fig. S11. Free-energy diagrams for ORR pathways in an alkaline medium on FeN_4 at U=0 V and U=0.57 V.

Table S1. Content of C, N and Fe measured by XPS analysis.

Element	Content (wt %)
C	92.89
N	5.14
Fe	1.96

Table S2. Comparison of ORR electrochemical performance of Fe-N*x*-CNFs with recently reported Fe-based ORR electrocatalysts in basic electrolyte (0.1 M KOH)

Catalysts	Diffusion limited current density (mA cm^{-2})/Pt-C	Half-wave potential (V *vs*. RHE)/Pt-C	References
Fe-N*x*-CNFs	**6.08/5.31**	**0.875/0.822**	**This work**
Fe–Nx/HPC	5.0/5.0	0.88/0.84	[1]
Fe@N-doped graphene	~6.34/~5.82	0.85/0.85	[2]
Fe–N–C-900-control	~5.64/~5.3	0.905/0.872	[3]
Ni-N_4/GHSs/Fe-N_4	6.0/5.79	0.83/0.86	[4]
Fe/Ni–N–C	5.76/5.13	0.861/0.83	[5]
Fe/Mn-Nx-C	5.7/5.3	0.88/0.85	[6]
Fe-ISAs/CN	~6.2/~6.3	0.90/~0.85	[7]
SA-Fe-HPC	5.4/5.0	0.89/0.84	[8]
Fe/OES		0.85/0.85	[9]
Ce/Fe-NCNW	~5.64/~5.68	0.915/0.866	[10]
M-Fe-NCNS	~4.3/~4.1	0.88/0.82	[11]
Fe SAs-N/C-20	~6.16/~5.33	0.909/0.85	[12]
S,N-Fe/N/C-CNT	6.68/~5.6	0.85/0.82	[13]
Fe SAs/N−C	5.75/5.56	0.91/0.842	[14]
Fe-SAs/NPS-HC	5.95/6.1	0.912/0.84	[15]
Fe-SAs/NSC	6/5.41	0.87/0.86	[16]
AC@f-FeCoNC900	~5.75/~5.5	0.89/0.84	[17]
Fe-N-CNTs-12	6.18/5.726	0.89/0.841	[18]
UNT Co SAs/N-C	~5.1/~4.7	~0.89/~0.88	[19]
Fe@N-C-12	~5.9/~6.3	20 mV positive than Pt/C	[20]
Fe-NCCs	~6.3/~6	0.82/0.84	[21]
Fe−N−C/rGO	~5.9/~6.1	0.81/0.82	[22]
Fe-ISAs@CN		0.854/0.842	[23]
Fe1-N-CNFs	~4.8/4.5	0.84/0.79	[24]

References

1 Z.P. Zhang, X.J. Gao, M.L. Dou, J. Ji, F. Wang, Fe–Nx moiety-modified hierarchically porous carbons derived from porphyra for highly effective oxygen reduction reaction, *J. Mater. Chem. A,* 2017, **5**, 1526–1532.

2 D. Liu, C. Wu, S. Chen, S. Ding, Y. Xie, C. Wang. T. Wang. Y.A. Haleem, Z.u. Rehman, Y. Sang, Q. Liu, X. Zheng, Y. Wang, B. Ge,H. Xu, L. Song. *In situ* trapped high-density single metal atoms within graphene: Iron-containing hybrids as representatives for efficient oxygen reduction, *Nano Res.*, 2018, **11(4)**, 2217–2228.

3 C. Zhu, Q. Shi, B.Z. Xu, S. Fu, G. Wan, C. Yang, S. Yao, J. Song, H. Zhou, D. Du, S.P. Beckman, D. Su, Y. Lin, Hierarchically Porous M–N–C (M = Co and Fe) Single-Atom Electrocatalysts with Robust MNx Active Moieties Enable Enhanced ORR Performance, *Adv. Energy Mater.,*2018, 1801956.

4 J. Chen, H. Li, C. Fan, Q. Meng, Y. Tang, X. Qiu,G. Fu, T. Ma, Dual Single-Atomic Ni-N_4 and Fe-N4 Sites Constructing Janus Hollow Graphene for Selective Oxygen Electrocatalysis, *Adv. Mater.*, 2020, 2003134.
5 H. Li, J. Wang, R. Qi, Y. Hu, J. Zhang, H. Zhao, J. Zhang, Y. Zhao, Enhanced Fe 3d delocalization and moderate spin polarization in Fe–Ni atomic pairs for bifunctional ORR and OER electrocatalysis, *Appli. Catal. B- Environ.,* 2021, **285**, 119778.
6 Z. Chen, X. Liao, C. Sun, K. Zhao, D. Ye, J. Li, G. Wu, J. Fang, H. Zhao, J. Zhang, Enhanced performance of atomically dispersed dual-site Fe-Mn electrocatalysts through cascade reaction mechanism, *Appli. Catal. B- Environ.*, 2021, **288**, 120021.
7 Y. Chen, S. Ji, Y. Wang, J. Dong, W. Chen, Z. Li, R. Shen, L. Zheng, Z. Zhuang, D. Wang, Y. Li, Isolated Single Iron Atoms Anchored on N-Doped Porous Carbon as an Efficient Electrocatalyst for the Oxygen Reduction Reaction, *Angew. Chem. Int. Ed.*, 2017, **56(24)**, 6937-6941.
8 Z. Zhang, J. Sun, F. Wang, L. Dai, Efficient Oxygen Reduction Reaction (ORR) Catalysts Based on Single Iron Atoms Dispersed on a Hierarchically Structured Porous Carbon Framework, *Angew. Chem.*, 2018, **130**, 9176 –9181.
9C.-C. Hou, L. Zou, L. Sun, K. Zhang, Z. Liu, Y. Li, C. Li, R. Zou, J. Yu, Q. Xu, Single-Atom Iron Catalysts on Overhang-Eave Carbon Cages for High-Performance Oxygen Reduction Reaction, *Angew. Chem. Int. Ed.* 2020, **59**, 7384-7389.
10 J.C. Li, S. Maurya, Y.S. Kim, T. Li, L. Wang, Q. Shi, D. Liu, S. Feng, Y. Lin, M. Shao, Stabilizing Single-Atom Iron Electrocatalysts for Oxygen Reduction via Ceria Confining and Trapping, *Acs Catal.*, 2020, **10(4)**, 2452-2458.
11 M. Wang, H. Ji, S. Liu, H. Sun, J. Liu, C. Yan, T. Qian, Single-atom scale metal vacancy engineering in heteroatom-doped carbon for rechargeable zinc-air battery with reduced overpotential, *Chem. Eng. J.,*2020, **393**, 124702.
12 R. Jiang, L. Li, T. Sheng, G. Hu, Y. Chen, L. Wang, Edge-Site Engineering of Atomically Dispersed Fe-N_4 by Selective C-N Bond Cleavage for Enhanced ORR Activities, *J. Am. Chem. Soc.*, 2018, **140**, 11594–11598.
13 P. Chen, T. Zhou, L. Xing, K. Xu, Y. Tong, H. Xie, L. Zhang, W. Yan, W. Chu, C. Wu, Y. Xie, Atomically Dispersed Iron–Nitrogen Species as Electrocatalysts for Bifunctional Oxygen Evolution and Reduction Reactions, *Angew. Chem. Int. Ed.,* 2017, **56**, 610–614.
14 Z. Yang, Y. Wang, M. Zhu, Z. Li, W. Chen, W. Wei, T. Yuan, Y. Qu, Q. Xu, C. Zhao, X. Wang, P. Li, Y. Li, Y. Wu, Y. Li, Boosting Oxygen Reduction Catalysis with Fe−N_4 Sites Decorated Porous Carbons toward Fuel Cells, *ACS Catal.,*2019, **9**, 2158−2163.
15 Y. Chen, S. Ji, S. Zhao, W. Chen, J. Dong, W.-C. Cheong, R. Shen, X. Wen, L. Zheng, A.I. Rykov, S. Cai, H. Tang, Z. Zhuang, C. Chen, Q. Peng, D. Wang, Y. Li, Enhanced oxygen reduction with single-atomic-site iron catalysts for a zinc-air battery and hydrogen-air fuel cell, *Nature Commun.*, 2018, **9**, 5422.
16 J. Zhang, Y. Zhao, C. Chen, Y.C. Huang, C.L. Dong, C.J. Chen, R.S. Liu, C. Wang, K. Yan, Y. Li, G. Wang, Tuning the Coordination Environment in Single-Atom Catalysts to Achieve Highly Efficient Oxygen Reduction Reactions, *J. Am. Chem. Soc.*, 2019, **141(51)**, 20118-20126.
17 G. Zhang, Y. Jia, C. Zhang, X. Xiong, K. Sun, R. Chen, W. Chen, Y. Kuang, L. Zheng, H. Tang, W. Liu, J. Liu, X. Sun, W.-F. Lin, H. Dai, A general route via for mamide condensation to prepare atomically dispersed metal–nitrogen–carbon electrocatalysts for energy technologies,

Energy Environ. Sci., 2019, **12**, 1317-1325.
18 Z. Zhang, H. Jin, J. Zhu, W. Li, C. Zhang, J. Zhao, F. Luo, Z. Sun, S. Mu, 3D flower-like ZnFe-ZIF derived hierarchical Fe, N-Co doped carbon architecture for enhanced oxygen reduction in both alkaline and acidic media, and zinc-air battery performance, *Carbon*, 2020, **161**, 502-509.
19 X. Sun, S. Sun, S. Gu, Z. Liang, J. Zhang, Y. Yang, Z. Deng, P. Wei, J. Peng, Y. Xu, C. Fang, Q. Li, J. Han, Z. Jiang, Y. Huang, High-performance single atom bifunctional oxygen catalysts derived from ZIF-67 superstructures, *Nano Energy*, 2019, **61**, 245-250.
20 Y. Ye, H. Li, F. Cai, C. Yan, R. Si, S. Miao, Y. Li, G. Wang, X. Bao, Two-Dimensional Mesoporous Carbon Doped with Fe−N Active Sites for Efficient Oxygen Reduction, *ACS Catal.*, 2017, **7**, 7638−7646.
21 N. Jia, Q. Xu, F. Zhao, H.-Xu Gao, J. Song, P. Chen, Z. An, X. Chen, Y. Chen, Fe/N Codoped Carbon Nanocages with Single-Atom Feature as Efficient Oxygen Reduction Reaction Electrocatalyst, *ACS Appl. Energy Mater.*, 2018, **1**, 4982−4990.
22 C. Zhang, J. Liu, Y. Ye, Z. Aslam, R. Brydson, C. Liang, Fe−N-Doped Mesoporous Carbon with Dual Active Sites Loaded on Reduced Graphene Oxides for Efficient Oxygen Reduction Catalysts, *ACS Appl. Mater. Interfaces*, 2018, **10**, 2423−2429.
23 W. Yang, P. Hong, D. Yang, Y. Yang, Z. Wu, C. Xie, J. He,K. Zhang, L. Kong, J. Liu, Enhanced Fenton-like degradation of sulfadiazine by single atom iron materials fixed on nitrogen-doped porous carbon, *J. Colloid Interf. Sci.*, 2021,**597**, 56-65.
24 L. Dong, J. Zang, W. Wang, X. Liu, Y. Zhang, J. Su, Y. Wang, X. Han, J. Li, Electrospun single iron atoms dispersed carbon nanofibers as high performance electrocatalysts toward oxygen reduction reaction in acid and alkaline media, *J. Colloid Interf. Sci.*, 2020, **564**, 134–142.